

Isolating the optical response of a MoS₂ monolayer under extreme screening of a metal substrate

Tao Yang ^{1,*}, Stephan Sleziona ¹, Erik Pollmann,¹ Eckart Hasselbrink ², Peter Kratzer ¹, Marika Schleberger ¹, R. Kramer Campen ¹ and Yujin Tong ^{1,†}

¹Faculty of Physics, University of Duisburg-Essen, 47057 Duisburg, Germany

²Faculty of Chemistry, University of Duisburg-Essen, 45117 Essen, Germany



(Received 31 October 2023; revised 13 March 2024; accepted 14 March 2024; published 12 April 2024)

Transition metal dichalcogenides (TMDCs) monolayers, as two-dimensional (2D) direct bandgap semiconductors, hold promise for advanced optoelectronic and photocatalytic devices. Interaction with three-dimensional (3D) metals, like Au, profoundly affects their optical properties, posing challenges in characterizing the monolayer's optical responses within the semiconductor-metal junction. In this study, using precise polarization-controlled final-state sum frequency generation (FS-SFG), we successfully isolated the optical responses of a MoS₂ monolayer from a MoS₂/Au junction. The resulting SFG spectra exhibit a linear lineshape, devoid of A or B exciton features, attributed to the strong dielectric screening and substrate induced doping. The linear lineshape illustrates the expected constant density of states (DOS) at the band edge of the 2D semiconductor, a feature often obscured by excitonic interactions in weak-screening conditions such as in a free-standing monolayer. Extrapolation yields the onset of a direct quasiparticle bandgap of about 1.65 ± 0.20 eV, indicating a strong bandgap renormalization. This study not only enriches our understanding of the optical responses of a 2D semiconductor in extreme screening conditions but also provides a critical reference for advancing 2D semiconductor-based photocatalytic applications.

DOI: [10.1103/PhysRevB.109.L161402](https://doi.org/10.1103/PhysRevB.109.L161402)

Introduction. The unique appeal of monolayers of transition metal dichalcogenides (TMDCs) lies in their distinctive characteristics as two-dimensional (2D) direct bandgap semiconductors [1,2]. The strong light-matter interaction and the quantum confinement effect position these materials as promising candidates for advancing next-generation optoelectronic and photocatalytic devices [3–6]. In light of these prospects, a fundamental question arises: How does a 2D TMDC monolayer maintain its semiconductor characteristics when interfaced with a three-dimensional (3D) metal? This query is pivotal, considering the well-known strong screening and doping effects associated with bulk metals. Beyond its fundamental implications, this question also holds practical relevance within the fields of TMDC-based 2D transistors [7–9] and photocatalysis [10–12]. However, the precise characterization of the electronic properties of a 2D semiconductor on a 3D metal substrate presents substantial challenges. Techniques such as scanning tunneling spectroscopy (STS) offer a means of gauging the electronic bandgap by monitoring the onset of tunneling current [13,14]. However, accurately determining the onset of tunneling current remains a non-trivial task, potentially introducing ambiguity in the derived bandgap energy [15]. An alternative approach involving time- and angle-resolved photoemission spectroscopy (tr-ARPES) shows promise for electronic bandgap determination [16,17]. However, the applicability of tr-ARPES is constrained by its demanding experimental requisites.

There is a well-established optical method in the device community, the Tauc plot, which has been used extensively to determine the bandgap of 3D amorphous semiconductors [18–20]. Originally, Tauc developed the expression $\sqrt{\alpha(E)\hbar\nu} \propto \hbar\nu - E_{opt}$ to determine the optical absorption edge for amorphous semiconductors, Ge and Si. Here $\alpha(E)$ denotes the absorption coefficient, $\hbar\nu$ the photon energy, and E_{opt} the optical bandgap. While this method may also be adapted for use with crystalline semiconductors such as thin layers of TMDCs after certain modifications, challenges arise due to the presence of excitonic features at the band edge. There is an ongoing debate regarding the construction of the Tauc plot for TMDC systems. Some studies involve drawing the slope from the lower-energy side of the A exciton [21,22], while others base it on the quasiparticle bandgap [23,24] and simply ignore the excitonic features. Clearly, the accurate characterization of the onset of the band edge of a TMDC monolayer depends on a comprehensive understanding of its optical properties under different environments.

Theoretically, a 2D semiconductor with direct bandgap is expected to have a constant, with respect to energy, density of states (DOS) at the band edges within a quasiparticle picture [20]. The optical response, which is directly related to the joint DOS, should increase linearly with photon energy due to the convolution of two constant functions. However, in most practical TMDC systems insufficient screening generally enhances the Coulomb interaction between the electrons and holes, leading to exciton formation and complicating interpretation of the observed lineshapes. Intriguingly, by placing the TMDC on a metal surface, it may be possible to recover the intrinsic exciton-free optical response of the 2D material.

*tao.yang@uni-due.de

†yujin.tong@uni-due.de

This suggests that it might be possible to extract the bandgap from linear extrapolation of the optical response in analogy to the Tauc plot. Regrettably, when the TMDC is positioned on a metal surface, it is extremely difficult to isolate its pure optical response from that of the underlying metallic substrate. For instance, in the case of a MoS₂ monolayer on Au, the photoluminescence (PL) signal is completely quenched [25,26]. While absorption or reflectivity measurements can still provide an optical response from the TMDC monolayer on a metal system, the large optical response from the free electrons of the substrate often obscures the optical response of the TMDC [27], even though some subtle features in the first derivative of the spectrum have been reported [28]. These persistent challenges impede a comprehensive understanding of the optical behavior of TMDC monolayers interfaced with a metal substrate.

Sum frequency generation (SFG) spectroscopy, a second-order nonlinear spectroscopic technique [29,30], offers sensitivity to the structural symmetry of MoS₂. In a prior study, we demonstrated the possibility of isolating the optical response of MoS₂ from that of the metal by leveraging their respective symmetries [31]. In this work, we extensively investigate the influence of a metallic substrate on the spectra of MoS₂. For the first time, a linear optical lineshape of the TMDC monolayer has been recovered at the band edge. This not only allows us to unambiguously conclude that the commonly observed A and B excitons disappear under such extreme screening and doping conditions, but also provides previously unrevealed information to discuss the unique electronic property of the TMDC monolayer in contact with metal with the help of density functional theory (DFT) calculations. Given the disappearance of the exciton features, we can derive an analogous Tauc plot method using the pure second-order nonlinear susceptibility ($\chi^{(2)}$) of MoS₂. With this method, we succeed in extracting the intrinsic bandgap (1.65 ± 0.20 eV) of MoS₂ within the semiconductor-metal junction, suggesting that a strong bandgap renormalization has been induced by the Au substrate. This study can be extended to other 2D semiconductor and 3D metal junctions which are commonly encountered in optoelectronic and photocatalytic devices. The information obtained can greatly improve our understanding of the optical properties of 2D semiconductors, especially in the presence of significant concentrations of free carriers.

Experimental details. In this study, we collected final-state sum frequency generation (FS-SFG) signals from a monolayer of MoS₂ on Au, where the Au film was deposited via physical vapor deposition (PVD). The MoS₂/Au sample was prepared through mechanical exfoliation of MoS₂ onto a freshly prepared Au surface [26]. For comparative analysis, we also investigated a monolayer of MoS₂ which was grown by chemical vapor deposition on a layer of silicon dioxide (SiO₂) on a silicon wafer [32,33]. Optical images of MoS₂/Au and MoS₂/SiO₂ can be referenced in Fig. S1 within the Supplemental Material [34]. A detailed depiction of the SFG experimental setup is provided in Fig. 1. Two laser beams were spatially and temporally overlapped on the sample surface, and the resulting emitted sum frequency photons were detected. The visible beam's photon energy was centered at 1.56 eV, while the photon energy of infrared (IR) beam

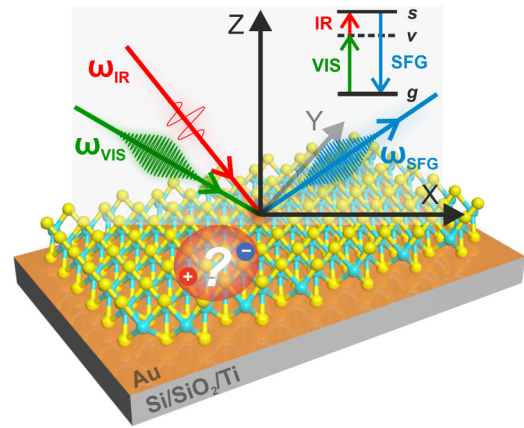


FIG. 1. Schematic representations of exfoliated MoS₂ monolayer on Au is investigated by the FS-SFG. Inset: Schematic energy level diagram of the FS-SFG, where g , v , and s represent the ground state, virtual state, and excited state, respectively. Only the SFG process will resonate with the excited state in the MoS₂ monolayer.

was tuned from 0.28–0.41 eV, ensuring that the final-state resonant SFG photon energies covered the A and B exciton energies. The visible beam energy was set at 0.8 μ J/pulse, and the infrared beam was maintained below 1.0 μ J/pulse. Both beams were propagated coplanarly with incident angles of 64° and 46° for the visible and infrared beams, respectively. The polarization of the three beams was individually set to p or s to obtain different polarization combinations, allowing us to choose the one best suited for the intended experiment. During measurements, azimuth-dependent patterns were initially obtained to guide the collection of FS-SFG spectra at specific azimuths, e.g., the angle with maximum intensity. A z -cut alpha quartz was used to obtain a reference signal for the purpose of correcting the frequency-dependent IR intensity. All experiments were conducted under ambient conditions at $\sim 21.5^\circ\text{C}$. Further details regarding the sample preparation, sample characterization, and the laser setup can be found in our previous work [26,35,36] and the Supplemental Material [34].

Results and discussion. To gain a basic overview of our samples, we initiated our study with Raman and PL measurements. As depicted in Fig. 2, both Raman and PL spectra

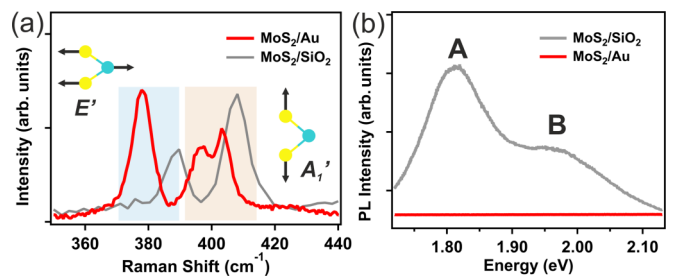


FIG. 2. (a) Raman spectra of MoS₂ monolayer on Au and Si/SiO₂ substrate. The inset illustrates two Raman-active modes (E' and A_1'). (b) PL spectra obtained at room temperature for MoS₂ monolayer on Au and Si/SiO₂ substrate with an excitation wavelength of 532 nm. The PL signal of MoS₂ on Au is strongly quenched.

of MoS₂ monolayers on Au and SiO₂ substrates manifest pronounced distinctions. Specifically, the Raman spectrum of the MoS₂ monolayer on SiO₂, as illustrated in Fig. 2(a), exhibits two notable peaks centered at 388.5 cm⁻¹ for the in-plane E' mode and 407.8 cm⁻¹ for the out-of-plane A_1' mode, respectively. The discernible 19.3 cm⁻¹ difference between these modes is characteristic of a monolayer structure [37]. However, the Raman spectrum of MoS₂ on Au showcases markedly different features. The E' mode undergoes a redshift to 377.9 cm⁻¹, and the A_1' mode exhibits a redshift and splits into two distinct peaks at 396.2 and 403.6 cm⁻¹. These changes align with earlier observations [26,38] and the lower A_1' mode can be attributed to the charge transfer from Au to the stretched MoS₂ layer [39].

The substantial interaction observed at the semiconductor-metal interface is further corroborated by the PL spectrum depicted in Fig. 2(b). The MoS₂ sample on SiO₂ exhibits distinctive features at 1.81 and 1.97 eV, corresponding to the A and B excitons of MoS₂, respectively. The presence of two excitons, A and B, originates from the splitting of the valence band maxima at the K point, induced by spin-orbit coupling [40]. In contrast, the PL signal from the MoS₂/Au sample is completely quenched (see Fig. S2 of the PL signal of MoS₂/Au with small intensity scale in the Supplemental Material [34]). These optical spectra are consistent with previous studies [26,38,41]. PL quenching has been reported previously [25] and was understood as the transfer of the photoexcited electron from the conduction band of MoS₂ to the Au substrate instead of undergoing radiation relaxation. This hypothesis is supported by tr-ARPES results, which demonstrate ultrafast dynamics of the photoexcited electrons relaxing back to Au [16]. However, the behavior of excitons within this heterointerface remained unclear. While there are reports claiming that the A and B excitons remain observable for MoS₂ on Au [28], others suggest a conclusion to the contrary [27]. The reason for the dispute is the weak signal of MoS₂, which is always hidden under the strong background signal of the Au substrate, making it difficult to unambiguously distinguish between them. Fortunately, second-order nonlinear spectroscopy techniques, such as FS-SFG, provide a unique opportunity to isolate the contribution of the monolayer semiconductor from that of the bulk substrate, capitalizing on their distinct symmetries. Further details regarding this isolation technique are elaborated below.

As demonstrated in earlier studies utilizing single-beam second harmonic generation (SHG), the 2H-MoS₂ monolayer is categorized under the D_{3h} point group, displaying a consistent sixfold symmetric pattern of SHG intensity [42–44]. Our recent investigation using SFG aligns with these prior findings and extends the understanding by revealing that the symmetric pattern of the MoS₂ monolayer on Au is highly dependent on polarization, resulting in a lowering of the symmetry to C_{3v} [31]. Within the C_{3v} point group, specific polarization combinations (e.g., spp , pps , psp , and sss , where spp indicates s polarized SFG, p polarized visible, and p polarized infrared beams) yield signals arising from only one azimuth-dependent second-order susceptibility component inherited from MoS₂. By carefully selecting the appropriate polarization combination, SFG enables selective investigation of the MoS₂ monolayer and provides the pure response from the

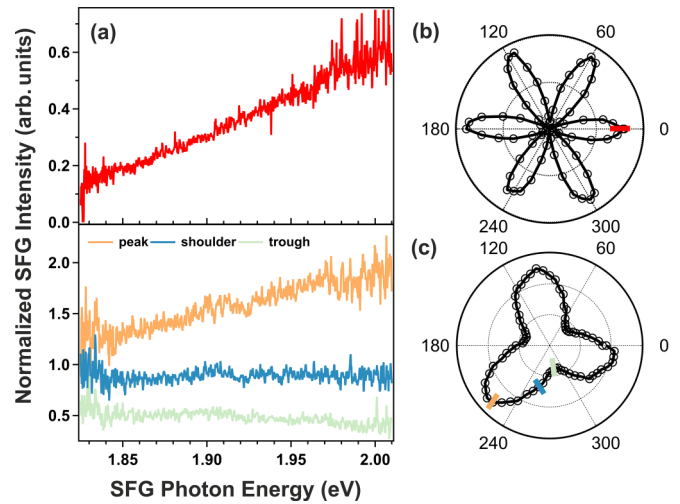


FIG. 3. (a) The normalized FS-SFG spectra of the MoS₂ monolayer on Au under spp (top) and ssp (bottom) polarization combinations. (b) and (c) are the azimuth-dependent SFG intensity of MoS₂/Au under spp and ssp polarization combination, respectively. There is a 13° offset in the azimuth between spp and ssp polarization combination. The spectra in (a) were collected at specific azimuths, marked in (b) and (c) with corresponding colors.

MoS₂ monolayer free from perturbations by the Au optical response.

The top and bottom panels in Fig. 3(a) show representative FS-SFG spectra of the MoS₂/Au sample under spp and ssp polarization combinations. The sharp peaks at the edges of the spectra in Fig. 3(a) are noise induced by spectrum normalization due to the lower output power of our laser system at the corresponding photon energy. Figures 3(b) and 3(c) are the corresponding azimuthal dependencies of the SFG intensity for the two polarization combinations. The azimuthal pattern for spp exhibits a sixfold symmetry, while that for ssp shows a threefold symmetry. The reason for the different azimuthal symmetric pattern has been extensively discussed in our previous work [31]. In brief, for spp polarization, the SFG signal purely originates from the MoS₂ layer, while both MoS₂ and Au contribute to the SFG signal when using ssp polarization. In the latter case, the interference of the two signals results in a reduction in the symmetry from sixfold to threefold. The relative ratio of two signals determines the shape of the petal in a threefold symmetric pattern.

In this work, we will focus on the spectra of these FS-SFG responses. For spp polarization combination, the spectral shape in the reported A and B exciton energy region is close to a straight line and the slope is independent of the azimuth, only the intensities change [Here only a representative spectrum collected at the maximum integrated FS-SFG intensities, which is marked in red in Fig. 3(b) is presented]. On the contrary, the spectral shape recorded under the ssp polarization combination [bottom panel of Fig. 3(a)] maintains a linear appearance, yet with slopes that exhibit significant sensitivity to the azimuth (the weak narrow features around 1.92 eV are from the vibrational responses of the unavoidable hydrocarbon impurities being upconverted by the 1.56 eV visible beam). Specifically, at the azimuthal intensity

maximum [highlighted in orange in Fig. 3(c)], the slope is positive; at the azimuthal intensity minimum [marked in light green in Fig. 3(c)], the slope is negative. Furthermore, at the shoulder, the spectrum appears nearly horizontal [indicated by the blue marker in Fig. 3(c)], akin to the FS-SFG response observed in pure PVD Au (refer to Fig. S3 in the Supplemental Material [34]). More details about the relationship between azimuth and spectral slope under *ssp* polarization can be found in the Supplemental Material [34]. To establish a reference, azimuth-dependent SFG intensity and the spectrum of MoS₂/SiO₂ were also obtained. A distinctive resonant peak is observed at ~ 1.84 eV, attributed to the A exciton, as illustrated in Fig. S4 of the Supplemental Material [34]. Clearly, in the case of MoS₂/Au, even though the FS-SFG photon energy falls within the A and B exciton energy range, all the spectra display a linear profile, and no excitonic features were observed.

While both the PL (Fig. 2) and the FS-SFG (Fig. 3) spectra suggest a quench of the excitonic features, the implications of the two observations differ significantly. The quenched spectrum in PL solely implies a nonradiative relaxation process, and it does not provide any additional information such as bandgap renormalization or potential substrate induced doping. On the contrary, the FS-SFG spectra of MoS₂ on Au distinctly exhibit the radiative signal. A comprehensive analysis of this signal can provide valuable insights into the electronic properties of this intricate system.

One of the intriguing properties of 2D materials is their extreme sensitivity to the screening from the environment. Both theory [45–47] and experiments [16,48] have shown that the screening from the environment or from the substrate doped free charge carriers inside the TMDC can effectively reduce the Coulomb interaction between electron-hole pairs, leading to an increase in their spatial separation and a reduction in the exciton's binding energy. Depending on the nature of screening (dynamic or static), the quasiparticle bandgap may be reduced (known as bandgap renormalization) by the same amount as the change of the binding energy of the exciton [46]. Obviously, metals possess an extremely large dielectric constant and produce a strong doping effect compared to free-standing or dielectric substrate-supported conditions. Consequently, stable excitons cannot be formed in a MoS₂ monolayer on Au at room temperature, as evidenced by our observation.

As the formation of excitons within MoS₂/Au is not feasible, the isolated optical response of the MoS₂ hence can report the electronic property of the semiconductor at the band edge, similar to the Tauc plot method reported for bulk amorphous semiconductors [19]. Figure 4 shows the results of such an analogous Tauc plot. A straight line is clearly obtained. Extrapolating the line in the plot to $|\chi_{\text{MoS}_2}^{(2)}| = 0$, as shown in Fig. 4, gives a value of 1.65 ± 0.20 eV as averaged from several independent measurements. Given that this response is approximately equivalent to the convolution of two constant DOS functions at the band edges (as confirmed by a DFT calculation), this value reports the onset of the bandgap at the *K* point in the first Brillouin zone (see Fig. S5 in the Supplemental Material [34] about the band structure and constant DOS).

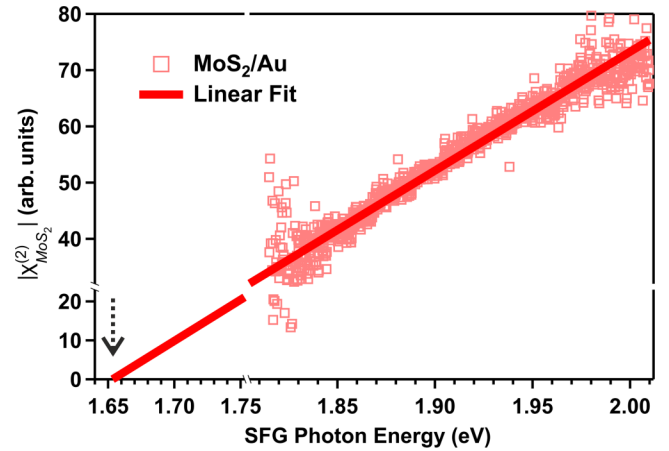


FIG. 4. The onset of bandgap in the MoS₂ monolayer on Au under *ssp* polarization combination was determined using the analogous Tauc plot method. A linear fit of the dependence of $|\chi_{\text{MoS}_2}^{(2)}|$ on the SFG photon energy was represented by the red solid line. The onset of the bandgap was extracted by extrapolating the linear fit to hit the energy axis ($|\chi_{\text{MoS}_2}^{(2)}| = 0$) and marked by an arrow.

The Tauc plot method has previously been utilized to determine the bandgap of TMDC thin films, without accounting for the impact of excitons [21,22]. However, for a free-standing TMDC monolayer or a monolayer on a dielectric substrate, the presence of excitons due to insufficient screening, can significantly hinder the unambiguous identification of the absorption edge. In contrast, in the current study, the exciton binding energy is sufficiently low when the TMDC monolayer is placed on Au, so that the analogous Tauc plot becomes possible as long as the pure monolayer response can be extracted. It should be noted that in this study we directly plot the Fresnel factor corrected $|\chi_{\text{MoS}_2}^{(2)}|$ as a function of the sum frequency photon energy, rather than plotting $|\alpha_{\text{MoS}_2} h\nu|^n$ as a function of the input photon energy $h\nu$ (see Fig. S6 in the Supplemental Material [34] for the Fresnel factor in the measured energy range). This approach is justified by the Miller theory in nonlinear optics [30], where the lineshapes of a final state resonance in a second-order nonlinear optical process are identical to those of a linear optical process such as optical absorption (see the Supplemental Material [34] for further discussion).

The quasiparticle bandgap determined in this investigation is notably reduced compared to that of a free-standing or dielectrically supported monolayer of MoS₂. Evidently, a pronounced bandgap renormalization has transpired. Comparable instances of bandgap renormalization phenomena have been reported in prior research [13,16]. A tr-ARPES study of MoS₂ monolayer on Au revealed a direct electronic bandgap of 1.95 eV at the *K* point [16]. However, it should be noted that the bandgap measured in their study refers to the energy difference between the center of the conduction band minimum and that of the valence band maximum at the *K* point, whereas the value extracted from our experiment is the difference between the valence band maximum and conduction band minimum energies. Considering the full width at the half maximum (~ 0.3 eV) of the bands in the tr-ARPES

results (Fig. 2 in Ref. [16]), our results are in agreement with theirs. In an STS study of MoS_2 monolayer on Au, a bandgap of 1.74 ± 0.27 eV was extracted from the STS spectra [13], aligning closely with our result. The phenomenon of bandgap renormalization can be comprehended as the result of screening effects arising from the substrate and additional charge carriers within the monolayer via substrate doping. It is imperative to acknowledge that quantifying the bandgap renormalization of a monolayer of TMDC through conventional optical measurements, such as PL or optical absorption, is generally unattainable. This constraint arises from the comparable magnitudes of the alterations in exciton binding energy and the redshift of the quasiparticle band gap. Consequently, minimal variation in optical transition energy occur across diverse carrier densities [15,17]. However, in the present investigation, the unequivocal observation of exciton disappearance allows us to present the findings depicted in Fig. 4, which reports on the bandgap renormalization. Additionally, different quasiparticle bandgap values, ranging from 1.6 to 2.9 eV, have been reported from previous calculations using different levels of theories [46,49,50]. Our results provide new and reliable parameters for future comparison between the theory and experiment.

The interfaces created when 2D semiconductors come into contact with 3D metallic electrodes play a pivotal role in many newly developed optoelectronic and photocatalytic devices [51,52]. Our study offers a straightforward optical method to characterize the optical response of the 2D semiconductor itself with a noncontact manner. Such a method can be extended to other similar systems for devices based on the optoelectronic properties of TMDCs.

While our current research is informative, it is important to acknowledge certain limitations. Specifically, the limited probing frequency range is a result of constraints imposed by our experimental setup. Additionally, in the determination of the bandgap onset using the analogous Tauc plot, we had to employ an approximation based on Miller's rule [30].

However, despite these constraints, our conclusions regarding the absence of A and B excitons and the observed reduction of the bandgap for MoS_2/Au are firmly rooted in the experimental data. To address these limitations and deepen our understanding, we plan to widen the optical window and conduct heterodyne SFG measurements in our future studies.

Conclusion. Through careful polarization selection in the FS-SFG measurements, we were able to effectively isolate the MoS_2 monolayer's optical response from the MoS_2/Au system. The significant screening effect induced by the Au substrate and by the doped free carriers inside the monolayer results in a substantial reduction of the exciton's binding energy, effectively impeding the formation of A and B excitons. Under these conditions, we could extract the expected linear onset of optical absorption of a TMDC semiconductor under a quasiparticle picture. Our study provides valuable insights for understanding the electronic properties at the 2D semiconductor and 3D metal junction with the help of DFT calculations. By introducing an analogous Tauc plot using the pure second-order nonlinear susceptibility ($|\chi_{\text{MoS}_2}^{(2)}|$), we accurately determine a quasiparticle bandgap of 1.65 ± 0.20 eV, and a strong bandgap renormalization has been revealed. This methodology can be applied to various 2D semiconductor and 3D metal junctions, improving our understanding of optical properties in the presence of abundant free carriers and providing a valuable reference for the further development of photocatalysts.

Acknowledgments. This work was funded by the Deutsche Forschungsgemeinschaft (DFG, German Research Foundation) through Projects A06, B02, and C05 within the SFB 1242 "Non-Equilibrium Dynamics of Condensed Matter in the Time Domain" (Project No. 278162697) and through Project No. 429784087, through Germany's Excellence Strategy (EXC 2033 - 390677874 - RESOLV). Additional support was provided by the European Research Council, i.e., ERC-CoG-2017 SOLWET (Project No. 772286) to R.K.C.

-
- [1] K. F. Mak, C. Lee, J. Hone, J. Shan, and T. F. Heinz, Atomically thin MoS_2 : A new direct-gap semiconductor, *Phys. Rev. Lett.* **105**, 136805 (2010).
- [2] A. Splendiani, L. Sun, Y. Zhang, T. Li, J. Kim, C.-Y. Chim, G. Galli, and F. Wang, Emerging photoluminescence in monolayer MoS_2 , *Nano Lett.* **10**, 1271 (2010).
- [3] Q. H. Wang, K. Kalantar-Zadeh, A. Kis, J. N. Coleman, and M. S. Strano, Electronics and optoelectronics of two-dimensional transition metal dichalcogenides, *Nat. Nanotechnol.* **7**, 699 (2012).
- [4] K. F. Mak and J. Shan, Photonics and optoelectronics of 2D semiconductor transition metal dichalcogenides, *Nat. Photon.* **10**, 216 (2016).
- [5] T. Mueller and E. Malic, Exciton physics and device application of two-dimensional transition metal dichalcogenide semiconductors, *npj 2D Mater. Appl.* **2**, 29 (2018).
- [6] Y. Liu, X. Duan, H.-J. Shin, S. Park, Y. Huang, and X. Duan, Promises and prospects of two-dimensional transistors, *Nature (London)* **591**, 43 (2021).
- [7] B. Radisavljevic, A. Radenovic, J. Brivio, V. Giacometti, and A. Kis, Single-layer MoS_2 transistors, *Nat. Nanotechnol.* **6**, 147 (2011).
- [8] Z. Yin, H. Li, H. Li, L. Jiang, Y. Shi, Y. Sun, G. Lu, Q. Zhang, X. Chen, and H. Zhang, Single-layer MoS_2 phototransistors, *ACS Nano* **6**, 74 (2012).
- [9] A. D. Bartolomeo, L. Genovese, F. Giubileo, L. Iemmo, G. Luongo, T. Foller, and M. Schleberger, Hysteresis in the transfer characteristics of MoS_2 transistors, *2D Mater.* **5**, 015014 (2017).
- [10] J. Shi, R. Tong, X. Zhou, Y. Gong, Z. Zhang, Q. Ji, Y. Zhang, Q. Fang, L. Gu, X. Wang, Z. Liu, and Y. Zhang, Temperature-mediated selective growth of MoS_2/WS_2 and WS_2/MoS_2 vertical stacks on Au foils for direct photocatalytic applications, *Adv. Mater.* **28**, 10664 (2016).
- [11] X. Guo, Q. Li, Y. Liu, T. Jin, Y. Chen, L. Guo, and T. Lian, Enhanced light-driven charge separation and H_2 generation efficiency in WSe_2 nanosheet-semiconductor nanocrystal heterostructures, *ACS Appl. Mater. Interfaces* **12**, 44769 (2020).

- [12] L. E. Strange, J. Yadav, S. Garg, P. S. Shinde, J. W. Hill, C. M. Hill, P. Kung, and S. Pan, Investigating the redox properties of two-dimensional MoS₂ using photoluminescence spectro-electrochemistry and scanning electrochemical cell microscopy, *J. Phys. Chem. Lett.* **11**, 3488 (2020).
- [13] A. Bruix, J. A. Miwa, N. Hauptmann, D. Wegner, S. Ulstrup, S. S. Grønberg, C. E. Sanders, M. Dendzik, A. Grubišić Čabo, M. Bianchi, J. V. Lauritsen, A. A. Khajetoorians, B. Hammer, and P. Hofmann, Single-layer MoS₂ on Au(111): Band gap renormalization and substrate interaction, *Phys. Rev. B* **93**, 165422 (2016).
- [14] C. C. Silva, D. Dombrowski, N. Atodiresei, W. Jolie, F. F. z. Hagen, J. Cai, P. T. P. Ryan, P. K. Thakur, V. Caciuc, S. Blügel, D. A. Duncan, T. Michely, T.-L. Lee, and C. Busse, Spatial variation of geometry, binding, and electronic properties in the Moiré superstructure of MoS₂ on Au(111), *2D Mater.* **9**, 025003 (2022).
- [15] G. Wang, A. Chernikov, M. M. Glazov, T. F. Heinz, X. Marie, T. Amand, and B. Urbaszek, Colloquium: Excitons in atomically thin transition metal dichalcogenides, *Rev. Mod. Phys.* **90**, 021001 (2018).
- [16] A. G. Čabo, J. A. Miwa, S. S. Grønberg, J. M. Riley, J. C. Johannsen, C. Cacho, O. Alexander, R. T. Chapman, E. Springate, M. Grioni, J. V. Lauritsen, P. D. C. King, P. Hofmann, and S. Ulstrup, Observation of ultrafast free carrier dynamics in single layer MoS₂, *Nano Lett.* **15**, 5883 (2015).
- [17] F. Liu, M. E. Ziffer, K. R. Hansen, J. Wang, and X. Zhu, Direct determination of band-gap renormalization in the photoexcited monolayer MoS₂, *Phys. Rev. Lett.* **122**, 246803 (2019).
- [18] J. Tauc, Optical properties and electronic structure of amorphous Ge and Si, *Mater. Res. Bull.* **3**, 37 (1968).
- [19] J. Klein, L. Kampermann, B. Mockenhaupt, M. Behrens, J. Strunk, and G. Bacher, Limitations of the tauc plot method, *Adv. Funct. Mater.* **33**, 2304523 (2023).
- [20] M. Grundmann, *The Physics of Semiconductors: An Introduction Including Nanophysics and Applications* (Springer, Berlin, Germany, 2016).
- [21] W. Zheng, M. Bonn, and H. I. Wang, Photoconductivity multiplication in semiconducting few-layer MoTe₂, *Nano Lett.* **20**, 5807 (2020).
- [22] A. Paul and I. Grinberg, Optical properties of MoS₂, MoSe₂, WS₂, and WSe₂ under external electric field, *Phys. Rev. Appl.* **17**, 024042 (2022).
- [23] M. Mattinen, T. Hatanpää, T. Sarnet, K. Mizohata, K. Meinander, P. J. King, L. Khriachtchev, J. Räsänen, M. Ritala, and M. Leskelä, Atomic layer deposition of crystalline MoS₂ thin films: New molybdenum precursor for low-temperature film growth, *Adv. Mater. Interfaces* **4**, 1700123 (2017).
- [24] S. Wang, J.-K. Huang, M. Li, A. Azam, X. Zu, L. Qiao, J. Yang, and S. Li, Growth of high-quality monolayer transition metal dichalcogenide nanocrystals by chemical vapor deposition and their photoluminescence and electrocatalytic properties, *ACS Appl. Mater. Interfaces* **13**, 47962 (2021).
- [25] U. Bhanu, M. R. Islam, L. Tetard, and S. I. Khondaker, Photoluminescence quenching in gold - MoS₂ hybrid nanoflakes, *Sci. Rep.* **4**, 5575 (2015).
- [26] E. Pollmann, S. Sleziona, T. Foller, U. Hagemann, C. Gorynski, O. Petri, L. Madau, L. Breuer, and M. Schleberger, Large-area, two-dimensional MoS₂ exfoliated on gold: Direct experimental access to the metal-semiconductor interface, *ACS Omega* **6**, 15929 (2021).
- [27] B. Zou, Z. Wu, Y. Zhou, Y. Zhou, J. Wang, L. Zhang, F. Cao, and H. Sun, Spectroscopic ellipsometry investigation of Au-assisted exfoliated large-area single-crystalline monolayer MoS₂, *Phys. Status Solidi RRL* **15**, 2100385 (2021).
- [28] S. Park, N. Mutz, T. Schultz, S. Blumstengel, A. Han, A. Aljarb, L.-J. Li, E. J. W. List-Kratochvil, P. Amsalem, and N. Koch, Direct determination of monolayer MoS₂ and WSe₂ exciton binding energies on insulating and metallic substrates, *2D Mater.* **5**, 025003 (2018).
- [29] Y. R. Shen, Surface properties probed by second-harmonic and sum-frequency generation, *Nature (London)* **337**, 519 (1989).
- [30] R. W. Boyd, *Nonlinear Optics* (Academic Press, 2020).
- [31] T. Yang, E. Pollmann, S. Sleziona, E. Hasselbrink, P. Kratzer, M. Schleberger, R. K. Campen, and Y. Tong, Interaction between a gold substrate and monolayer MoS₂: An azimuthal-dependent sum frequency generation study, *Phys. Rev. B* **107**, 155433 (2023).
- [32] E. Pollmann, L. Madau, S. Schumacher, U. Kumar, F. Heuvel, C. vom Ende, S. Yilmaz, S. Güngörmüs, and M. Schleberger, Apparent differences between single layer molybdenum disulphide fabricated via chemical vapour deposition and exfoliation, *Nanotechnology* **31**, 505604 (2020).
- [33] E. Pollmann, A. Maas, D. Marnold, A. Hucht, R.-M. Neubieser, M. Stief, L. Madau, and M. Schleberger, Dynamic growth/etching model for the synthesis of two-dimensional transition metal dichalcogenides via chemical vapour deposition, *2D Mater.* **9**, 035001 (2022).
- [34] See Supplemental Material at <http://link.aps.org/supplemental/10.1103/PhysRevB.109.L161402> for experimental and theoretical information, which includes the optical images of the samples, normalized SFG spectra of PVD Au and MoS₂/SiO₂, details about sample preparation and laser setup, DFT-calculated band structure and density of states of MoS₂ monolayer on Au, and calculated Fresnel factor. Furthermore, we include justification of using $|\chi^{(2)}|$ to characterize the band edge.
- [35] Y. Tong, F. Lapointe, M. Thämer, M. Wolf, and R. K. Campen, Hydrophobic water probed experimentally at the gold electrode/aqueous interface, *Angew. Chem., Int. Ed.* **56**, 4211 (2017).
- [36] Y. Tong, I. Y. Zhang, and R. K. Campen, Experimentally quantifying anion polarizability at the air/water interface, *Nat. Commun.* **9**, 1313 (2018).
- [37] C. Lee, H. Yan, L. E. Brus, T. F. Heinz, J. Hone, and S. Ryu, Anomalous lattice vibrations of single- and few-layer MoS₂, *ACS Nano* **4**, 2695 (2010).
- [38] M. Velický, A. Rodríguez, M. Bouša, A. V. Krayev, M. Vondráček, J. Honolka, M. Ahmadi, G. E. Donnelly, F. Huang, H. D. Abruña, K. S. Novoselov, and O. Frank, Strain and charge doping fingerprints of the strong interaction between monolayer MoS₂ and gold, *J. Phys. Chem. Lett.* **11**, 6112 (2020).
- [39] S. Sarkar and P. Kratzer, Signatures of the dichalcogenide-gold interaction in the vibrational spectra of MoS₂ and MoSe₂ on Au(111), *J. Phys. Chem. C* **125**, 26645 (2021).
- [40] D. Xiao, G.-B. Liu, W. Feng, X. Xu, and W. Yao, Coupled spin and valley physics in monolayers of MoS₂ and other group-VI dichalcogenides, *Phys. Rev. Lett.* **108**, 196802 (2012).
- [41] N. Scheuschner, O. Ochedowski, A.-M. Kaulitz, R. Gillen, M. Schleberger, and J. Maultzsch, Photoluminescence of free-

- standing single- and few-layer MoS_2 , *Phys. Rev. B* **89**, 125406 (2014).
- [42] N. Kumar, S. Najmaei, Q. Cui, F. Ceballos, P. M. Ajayan, J. Lou, and H. Zhao, Second harmonic microscopy of monolayer MoS_2 , *Phys. Rev. B* **87**, 161403(R) (2013).
- [43] L. M. Malard, T. V. Alencar, A. P. M. Barboza, K. F. Mak, and A. M. de Paula, Observation of intense second harmonic generation from MoS_2 atomic crystals, *Phys. Rev. B* **87**, 201401(R) (2013).
- [44] T. Jiang, H. Liu, D. Huang, S. Zhang, Y. Li, X. Gong, Y.-R. Shen, W.-T. Liu, and S. Wu, Valley and band structure engineering of folded MoS_2 bilayers, *Nat. Nanotechnol.* **9**, 825 (2014).
- [45] T. Olsen, S. Latini, F. Rasmussen, and K. S. Thygesen, Simple screened hydrogen model of excitons in two-dimensional materials, *Phys. Rev. Lett.* **116**, 056401 (2016).
- [46] M. Drüppel, T. Deilmann, P. Krüger, and M. Rohlfing, Diversity of trion states and substrate effects in the optical properties of an MoS_2 monolayer, *Nat. Commun.* **8**, 2117 (2017).
- [47] A. Steinhoff, T. O. Wehling, and M. Rösner, Frequency-dependent substrate screening of excitons in atomically thin transition metal dichalcogenide semiconductors, *Phys. Rev. B* **98**, 045304 (2018).
- [48] M. M. Ugeda, A. J. Bradley, S.-F. Shi, F. H. da Jornada, Y. Zhang, D. Y. Qiu, W. Ruan, S.-K. Mo, Z. Hussain, Z.-X. Shen, F. Wang, S. G. Louie, and M. F. Crommie, Giant bandgap renormalization and excitonic effects in a monolayer transition metal dichalcogenide semiconductor, *Nat. Mater.* **13**, 1091 (2014).
- [49] T. Cheiwchanchamnangij and W. R. L. Lambrecht, Quasiparticle band structure calculation of monolayer, bilayer, and bulk MoS_2 , *Phys. Rev. B* **85**, 205302 (2012).
- [50] A. Kormányos, G. Burkard, M. Gmitra, J. Fabian, V. Zólyomi, N. D. Drummond, and V. Fal'ko, $k \cdot p$ theory for two-dimensional transition metal dichalcogenide semiconductors, *2D Mater.* **2**, 022001 (2015).
- [51] Y. Wang, J. C. Kim, R. J. Wu, J. Martinez, X. Song, J. Yang, F. Zhao, A. Mkhoyan, H. Y. Jeong, and M. Chhowalla, Van der Waals contacts between three-dimensional metals and two-dimensional semiconductors, *Nature (London)* **568**, 70 (2019).
- [52] P.-C. Shen, C. Su, Y. Lin, A.-S. Chou, C.-C. Cheng, J.-H. Park, M.-H. Chiu, A.-Y. Lu, H.-L. Tang, M. M. Tavakoli, G. Pitner, X. Ji, Z. Cai, N. Mao, J. Wang, V. Tung, J. Li, J. Bokor, A. Zettl, C.-I. Wu *et al.*, Ultralow contact resistance between semimetal and monolayer semiconductors, *Nature (London)* **593**, 211 (2021).